doi:10.1016/j.jmb.2009.07.033 J. Mol. Biol. (2009) 392, 723–735

JMB

Available online at www.sciencedirect.com

ScienceDirect

ELSEVIER

Multiple Metal-Binding Cores Are Required for Metalloregulation by M-box Riboswitch RNAs

Catherine A. Wakeman, Arati Ramesh and Wade C. Winkler*

Department of Biochemistry, The University of Texas Southwestern Medical Center, Dallas, TX 75390, USA

Received 3 April 2009; received in revised form 8 July 2009; accepted 11 July 2009
Available online 17 July 2009

Riboswitches are regulatory RNAs that control downstream gene expression in response to direct association with intracellular metabolites or metals. Typically, riboswitch aptamer domains bind to a single small-molecule metabolite. In contrast, an X-ray crystallographic structural model for the M-box riboswitch aptamer revealed the absence of an organic metabolite ligand but the presence of at least six tightly associated magnesiums. This observation agrees well with the proposed role of the M-box riboswitch in functioning as a sensor of intracellular magnesium, although additional nonspecific metal interactions are also undoubtedly required for these purposes. To gain greater functional insight into the metalloregulatory capabilities of M-box RNAs, we sought to determine whether all or a subset of the RNA-chelated magnesium ions were required for riboswitch function. To accomplish this task, each magnesium-binding site was simultaneously yet individually perturbed through random incorporation of phosphorothioate nucleotide analogues, and RNA molecules were investigated for their ability to fold in varying levels of magnesium. These data revealed that all of the magnesium ions observed in the structural model are important for magnesium-dependent tertiary structure formation. Additionally, these functional data revealed a new core of potential metal-binding sites that are likely to assist formation of key tertiary interactions and were previously unobserved in the structural model. It is clear from these data that M-box RNAs require specific binding of a network of metal ions for partial fulfillment of their metalloregulatory functions.

Keywords: nucleotide analogue interference mapping; noncoding RNA; riboswitch; magnesium–RNA interaction; RNA folding

Edited by D. E. Draper

Introduction

RNA molecules rely on intracellular metal ions for their structural and functional capabilities. Metal ions associate with RNA polymers to promote secondary structure by offsetting the electrostatic penalty incurred in bringing together backbone phosphates. In some cases, these ions may also bridge distantly located regions of an RNA molecule by forming specific and direct interactions to RNA functional groups. In general, monovalent ions encourage secondary structure formation, while divalent ions are more important for promoting tertiary structure.[1–5] Magnesium and potassium are the most common divalent and monovalent ions to associate with RNAs, respectively. In either instance, metal ions can bind tightly within RNA structures or remain loosely and nonspecifically associated. Magnesiums that chelate directly to RNA molecules are coordinated by three major functional groups: nonbridging phosphate oxygens, ribose oxygens, and nucleobase functional groups (e.g., guanine O6 carbonyls, N7 of purines, and pyrimidine O4 groups).[1,3,6] These tightly associated metal ions are oftentimes essential for formation of commonly observed RNA folds and motifs and assist in formation of complex RNA architectures.

One class of RNA elements that requires a high degree of structural complexity is referred to as riboswitches. Riboswitches are *cis*-acting regulatory RNA elements found within the untranslated regions of the mRNA transcripts that they regulate. Genetic

*Corresponding author. E-mail address: wade.winkler@utsouthwestern.edu.

Abbreviations used: EDTA, ethylenediaminetetraacetic acid; SAFA, semi-automated footprinting analysis.

regulation is accomplished through conformational changes that occur when riboswitch RNAs bind to their cognate ligands.[7–11] All of these RNAs contain a distinct aptamer domain, which is responsible for ligand binding and undergoes a conformational change that modulates downstream genetic regulatory features. This ligand-induced control of mutually exclusive riboswitch structures can be coupled to control of gene expression through modulation of transcription attenuation,[12,13] translation initiation,[14] mRNA stability,[15] or alternative splicing.[16,17]

Riboswitches have been discovered to respond to a variety of small organic metabolites including amino acids, nucleobases, nucleosides, enzymatic cofactors, an amino sugar, and a bacterial second messenger molecule.[11,18] Additionally, two riboswitch classes have been proposed to function as direct sensors of intracellular magnesium.[19,20] While metalloregulatory functions have previously been ascribed only to proteins, the later discoveries demonstrate that RNA polymers can also function as metal-sensing regulatory agents. One of these riboswitch classes, referred to as M-box RNAs,[20] has proved to be a particularly useful model for mechanistic analyses of metal-sensing regulatory RNAs. This RNA appears to play an important role in maintaining magnesium homeostasis in a variety of microorganisms. Within these organisms, M-box RNAs mostly regulate the expression levels of the three major families of magnesium transporters: CorA, MgtE, and MgtA/MgtB P-type ATPase proteins; however, in certain instances, they regulate additional protein classes whose roles in metal ion homeostasis have not yet been elucidated.[20]

Biochemical and biophysical analyses of the M-box riboswitch revealed that binding of divalent ions leads to formation of a compact tertiary architecture. This magnesium-bound compacted conformation results in sequestration of an oligonucleotide stretch within the aptamer domain, which prevents formation of an antiterminator helix and allows instead an intrinsic terminator helix to decrease downstream mRNA synthesis (Fig. 1a). A 2.7-Å structural model of

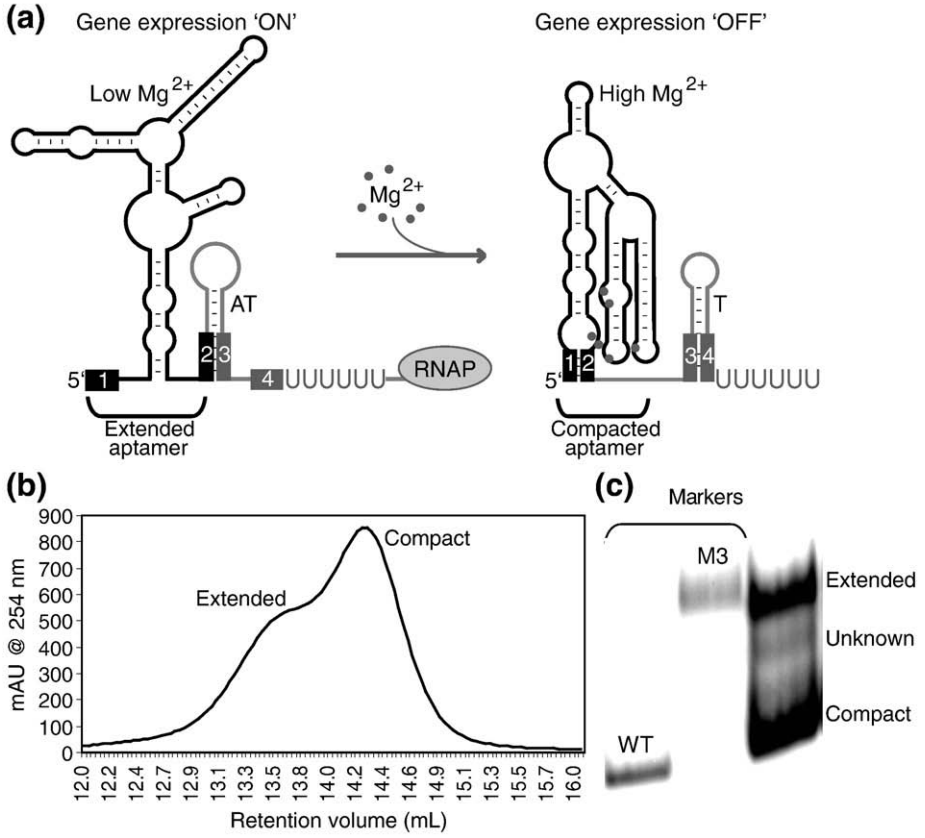

Fig. 1. Separation of extended and compact M-box RNAs. (a) Schematic showing the transition from extended to compact conformations for the M-box. Nucleotide stretches labeled 1–4 are regions that form base-pairing interactions such that downstream expression is 'on' in the unbound state and 'off' in the magnesium-bound state. Control of gene expression is achieved through mutually exclusive formation of either an intrinsic transcription terminator helix ("T") or an antiterminator helix ("AT"). The portion of the RNA colored black represents the aptamer domain that is responsible for ligand binding. RNAP, RNA polymerase. (b) Representative elution profile for size-exclusion chromatography in buffer containing 0.5 mM magnesium for M-box RNAs randomly modified at adenosines with phosphorothioate substitutions. (c) Nondenaturing gel electrophoresis of extended and compacted M-box species in the presence of 0.5 mM magnesium. WT (wild-type) and M3[20] mark the compact and extended states, respectively. A faint band labeled 'unknown' was observed to migrate between extended and compact RNA species. This newly identified species may require a distinct subset of the magnesium-binding sites (data not shown) and may represent a folding intermediate or a misfolded conformation.

the magnesium-bound M-box aptamer revealed the presence of at least six well-ordered magnesium ions interspersed throughout the RNA.[20] Presumably, this arrangement allows for cooperative binding of magnesiums and may assist genetic control over a more narrow range of ligand concentration than for noncooperative riboswitches. Cooperative binding of riboswitch ligands was also observed for glycine-sensing RNAs, which utilize a tandem arrangement of glycine-binding aptamer domains.[21] However, unlike the glycine riboswitch, M-box RNAs bind multiple ligand molecules within a single aptamer domain. Understanding the molecular basis for this metal ion network is critical for understanding M-box metallosensory function. Although most structurally complex RNAs also bind to magnesium, at least two other unrelated classes of riboswitches appear to be conformationally altered by magnesium over a ~100-fold range, likely making these RNAs relatively insensitive to small fluctuations in intracellular magnesium.[4] In contrast, M-box RNAs appear to be capable of responding to small (2- to 3-fold) changes in magnesium concentration. While the structural model derived by X-ray crystallography gives some insight into the molecular features that govern these characteristics, it is still likely to represent an incomplete portrayal. Indeed, the structural model provides a useful but static three-dimensional image of the final, magnesium-bound molecule. These data yield little information on the structural and molecular requirements during RNA folding or the importance of diffusely associated metal ions. To gain greater insight into their molecular mechanisms, M-box RNAs were subjected to analysis by nucleotide analogue interference mapping, a chemogenetic approach for studying functionally required features at an atomic level.[22–24]

Most inner-sphere interactions to magnesium occur through nonbridging phosphate oxygens. Random atomic substitution of phosphate oxygens for sulfur can then be used to abrogate binding of certain magnesiums due to the fact that 'hard' metals (e.g., magnesium) prefer to interact with 'hard' rather than 'soft' ligands (e.g., sulfur).[25] Therefore, sulfur substitutions at metal sites that are important for the compact conformation of M-box RNAs will result in RNA molecules trapped in the 'extended' state. While in some cases, interferences may simply occur due to steric effects caused by incorporation of the bulkier sulfur group,[26,27] phosphorothioate modifications are considered to be generally useful in studying essential magnesium–RNA contacts. Herein we identified phosphorothioate interference sites for an M-box RNA from *B. subtilis*. These sites cluster into three separate regions within the RNA. Two of these regions had been shown by prior structural analyses to be metal-binding cores and are functionally confirmed by data herein. A third potential metal-binding core was unidentified by the prior structural studies but revealed as important for tertiary structure formation by phosphorothioate mapping. In total, phosphorothioate interference analyses suggest that M-box RNAs utilize a complex network of direct metal-binding sites in order to exert metalloregulatory control.

Results

Separation of extended and compacted M-box RNAs

Nucleotide analogue interference mapping was used in this study to assess the relationship between divalent ions and nonbridging phosphate oxygens for M-box RNAs. Specifically, populations of RNA molecules containing random phosphorothioate substitutions were synthesized and functionally separated into pools of magnesium-bound and unbound RNAs. Previous studies have demonstrated that the M-box riboswitch undergoes molecular compaction upon association with magnesium, resulting in a significant reduction in molecular radius in the magnesium-bound state (Fig. 1a–c).[20] We exploited this magnesium-induced change in molecular shape for the separation of extended and compacted complexes by size-exclusion chromatography. Specifically, single phosphorothioate modifications were randomly incorporated into M-box RNAs during *in vitro* transcription, and the resulting RNA molecules were subjected to chromatographic separation in the presence of magnesium (Fig. 1b). Most phosphorothioate substitutions were neutral; correspondingly, most RNAs co-migrated with the magnesium-compacted conformation. However, an overlapping peak was observed that exhibited a retention volume matching RNAs trapped in the extended conformation. RNA molecules corresponding to both peaks were collected, radioactively labeled at the 5′ terminus, and further resolved by nondenaturing polyacrylamide gel electrophoresis in the presence of magnesium (i.e., native PAGE) (Fig. 1c). During native PAGE, the RNA pools were electrophoresed alongside wild-type RNAs to mark the location of the magnesium-bound, compact conformation and alongside a previously characterized mutant, 'M3',[20] to mark the location of the extended conformation. These experiments were separately performed for RNA molecules incubated in the presence of 0.5 mM magnesium, which is close to the magnesium concentration that triggers half-maximal compaction,[20] and 1.0 mM magnesium.

Phosphorothioate interferences at previously established magnesium-binding sites

To identify sites of sulfur substitution, phosphorothioate linkages were cleaved via iodine oxidation[28] and the RNA fragments were analyzed by denaturing PAGE (Supplementary Figs. S1 and S2). Sulfur modifications that were detrimental to a particular conformational state resulted in fainter bands as compared to the parent pool of RNA molecules, in which the extended and compacted species were not separated. Conversely, sites of phosphorothioate enhancement exhibited greater band intensity as

compared to the unselected pool. For analysis of phosphorothioate-substituted M-box RNAs, interference values were calculated from the ratio of band intensities for functionally separated RNAs and the unseparated, parent pool. These values were then normalized to account for minor loading differences (details can be found in Materials and Methods; Fig. 2a and b). In this study, interferences were grouped into three categories: strong interferences (interference values > 10), moderate interferences (interference values = 5–10), and weak but reproducible interferences (interference values = 2–5). Nucleotide positions at which phosphorothioate substitutions have virtually no effect have an interference value of approximately 1 in this analysis.

The six metal-binding sites (labeled as Mg1–Mg6) identified by prior structural analysis of the *B. subtilis mgtE* M-box RNA were proposed to incorporate a total of 12 inner-sphere interactions between divalent ions and RNA oxygens, occurring mostly between magnesiums and pro-R_p nonbridging phosphate oxygens. Based on our functional analysis, seven of these inner-sphere interactions, representing all of the known pro-R_p oxygen inner-sphere coordinations, were detected as sites of phosphorothioate interference when the RNA molecules were separated into extended and compacted pools in the presence of 0.5 mM magnesium (Fig. 3). Moreover, at least one deleterious sulfur substitution was observed for each of the six metal sites, indicating that all of the crystallographically observed divalents are required for metalloregulatory function.

Particularly strong interferences were observed at phosphate oxygens located 5′ of U24, G100, C102, A103, and G157, which together interact with three of the six ions (Mg1–Mg3). Notably, all three of the phosphate oxygen contacts to Mg1 are sites of strong interference (G100, C102, and A103), implicating Mg1 as a particularly important ion for the compacted state. Mg2 is coordinated by G157 through a magnesium-chelated water molecule. While phosphorothioate substitutions typically interfere with inner-sphere coordination of magnesium–oxygen interactions, phosphorothioate disruption of outer-sphere magnesium–RNA interactions have also been observed,[26] offering an explanation for the strong interference at G157. U23 and G100 form inner-sphere contacts to Mg2 via their pro-S_p phosphate oxygens, but the importance of these contacts could not be investigated in these experiments due to the fact that T7 RNA polymerase preferentially inserts phosphorothioate modifications in a pro-R_p configuration.[29] Moderate interferences were observed for 5′ phosphates of A72 and A63 contacting Mg4 and Mg5, respectively, suggesting an important but less critical role for these magnesiums. Finally, a weak but

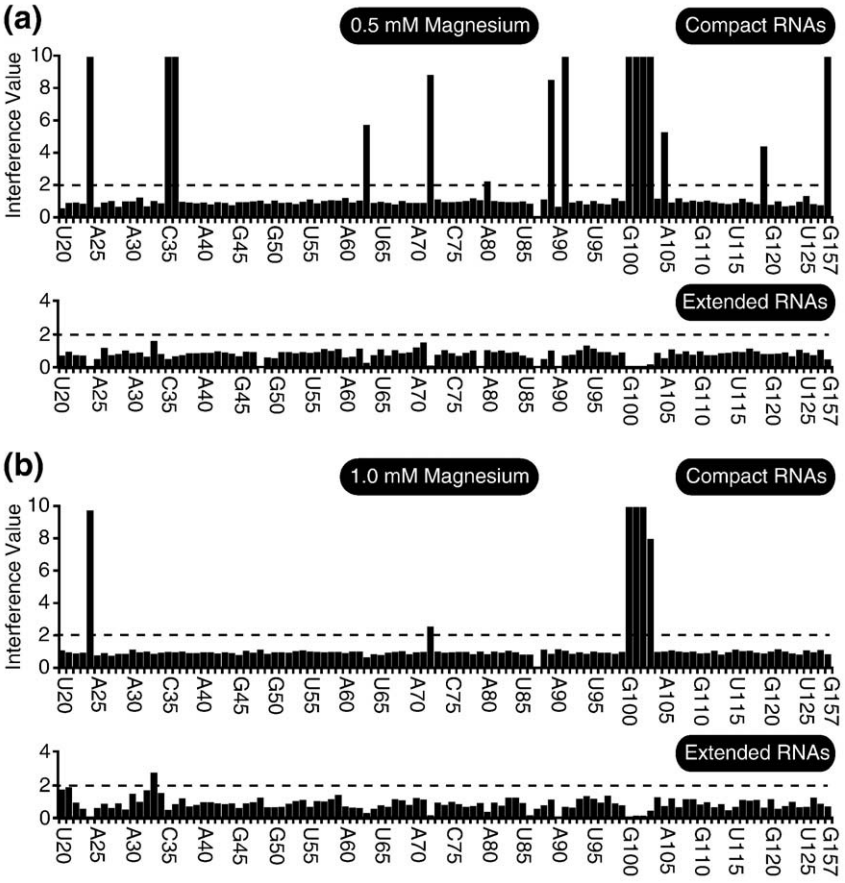

Fig. 2. Quantification of interference values for extended and compact M-box RNAs separated under (a) 0.5 mM and (b) 1.0 mM magnesium conditions. The dashed line indicates an arbitrary cutoff for interference values greater than 2.

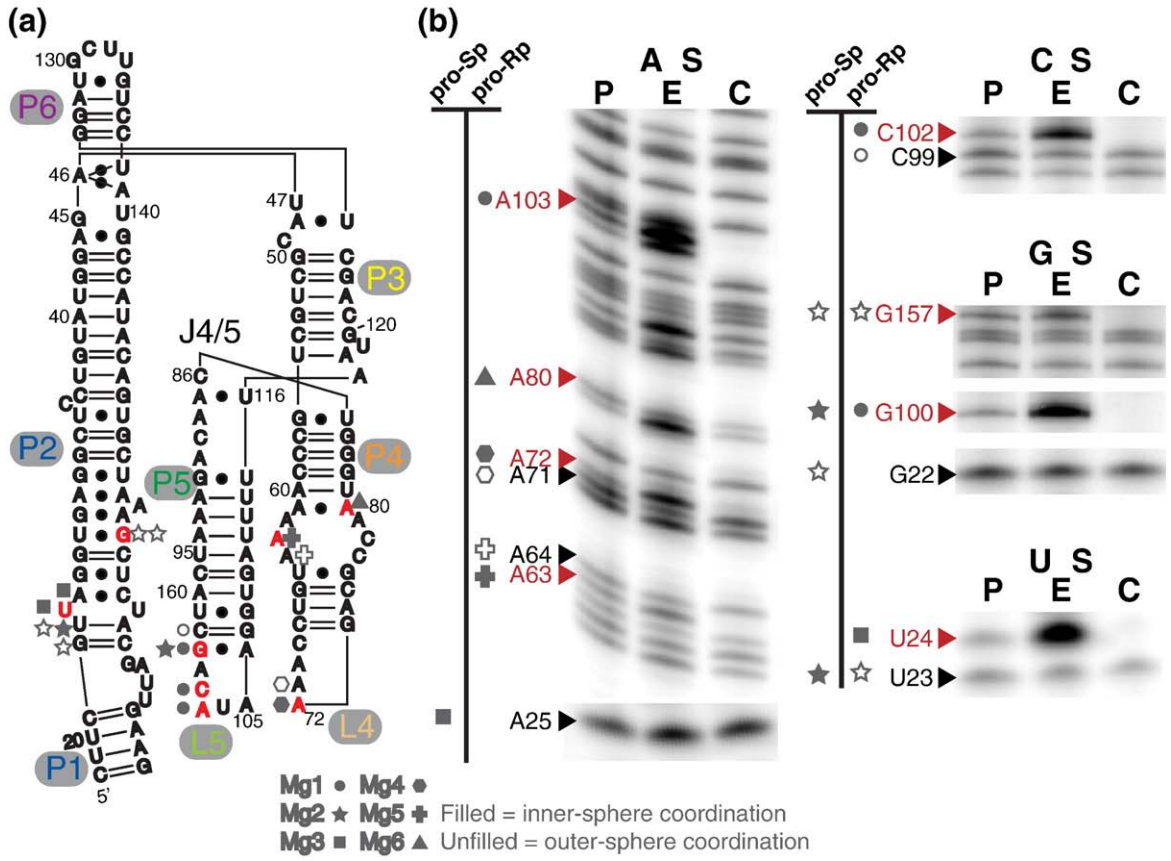

Fig. 3. Sites of phosphorothioate interferences at established magnesium-binding sites. (a) Secondary-structure diagram for the *B. subtilis mgtE* M-box RNA. Positions identified in the structural model[20] as coordinating to magnesiums (Mg1–Mg6) via phosphate oxygens are denoted by different symbols. The different helical elements and terminal loops are indicated with colored labels according to a color scheme utilized by the other figures in this article. Red letters denote positions of phosphorothioate interferences. (b) Representative data showing sites of phosphorothioate interferences for RNA molecules in 0.5 mM magnesium. P, parental, unselected transcription reaction; E, extended RNA molecules; C, compact RNAs. In most cases, individual phosphorothioate interferences for compact RNAs correlated with phosphorothioate enhancements for extended RNAs relative to the parental transcription pool. Symbols corresponding to Mg1–Mg6 are grouped into columns based on whether the metal coordinates to either the pro-S_p or the pro-R_p oxygen in the structural model.

reproducible interference was observed at the 5′ phosphate of A80, which contacts Mg6. In total, these biochemical data confirm the importance of all of the metal sites that were predicted by prior structural analyses.

When the RNA molecules were separated into extended and compacted pools in the presence of 1.0 mM magnesium, interferences at positions coordinating only three of the six known magnesium ions were observed (Mg1, Mg3, and Mg4), suggesting that metal excess can bypass the requirement for certain magnesium sites (Fig. 2b; Supplementary Fig. S2). At this concentration, strong interferences were observed at linkages responsible for coordinating Mg1 (G100, C102, and A103) and Mg3 (U24). Also, a weak but reproducible interference occurred for the 5′ phosphate of A72, which contacts Mg4.

Sites of additional phosphorothioate interferences

In addition to phosphorothioate interferences that corroborate crystallographically predicted magnesium-binding sites, strong interferences were also measured for compact RNAs at the 5′ phosphates of C35, C36, G91, and A101. Moderate interferences were also measured for C89 and A105, and a weak but reproducible interference was measured for U119 when the RNA pools were separated under 0.5 mM magnesium conditions (Fig. 4a). None of these sites correlate with known metal-binding sites, yet their locations within the structural model have allowed us to propose explanations for their importance in metal-mediated compaction. One exception is a weak but reproducible interference that appears in the extended RNA pool at position C33, which is more difficult to explain. Previous studies have noted that individual phosphorothioate substitutions can stabilize formation of certain, unfavored RNA structures.[30] The interference at C33 for extended RNAs may similarly result from stabilization of an alternate, unidentified state that is slightly favored over the extended conformation upon incorporation of the C33 phosphorothioate.

Interferences at A101 and A105 occur within the L5 terminal loop, which is responsible for construction of

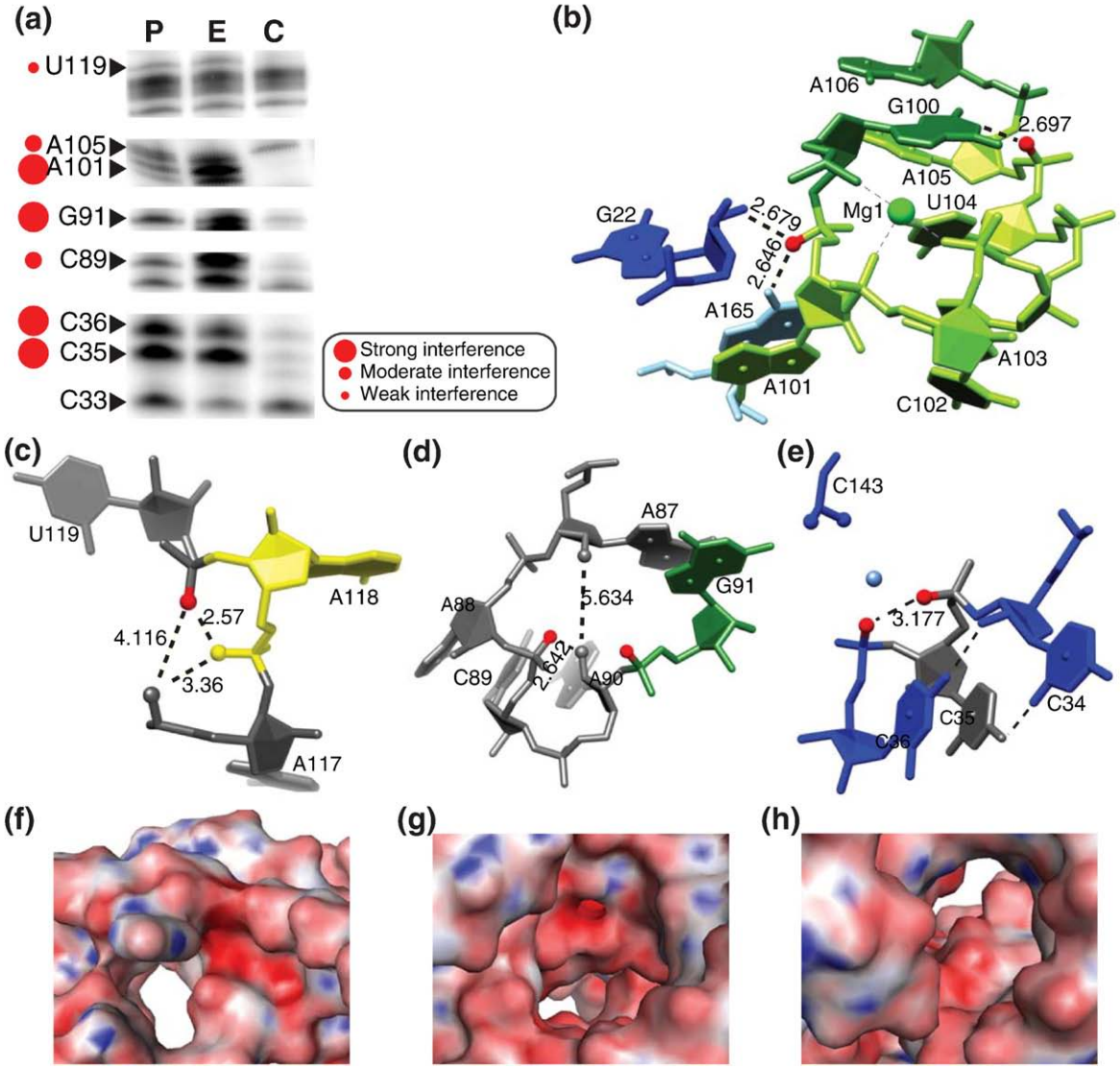

Fig. 4. Phosphorothioate interferences at positions not previously identified as magnesium-binding sites. (a) Representative data showing sites of phosphorothioate interferences for RNA molecules in 0.5 mM magnesium. P, parental, unselected transcription reaction; E, extended RNA molecules; C, compact RNAs. Strong interferences are marked by large circles, moderate interferences by medium-sized circles, and weak interferences by small circles. (b) Phosphorothioate modifications (shown with red spheres) at A101 and A105 are to likely interfere with formation of structural features required for the Mg1 binding site and interactions between L5 and P2. Black dashed lines denote putative hydrogen-bonding interactions disrupted by phosphorothioate substitutions. The green sphere represents Mg1. (c) Structural context for the phosphorothioate interference at the pro-R_p of U119. The pro-S_p phosphate oxygens of A117 and A118 and the U119 pro-R_p oxygen appear to coordinate formation of a candidate metal-binding site (M7). (d) Structural context for the phosphorothioate interferences at the pro-R_ps of C89 and G91, which may participate in formation of a metal-binding site (M8). (e) Structural context for phosphorothioate interferences at the pro-R_ps of C35 and C36, which may participate in formation of a metal-binding site (M9). Phosphate oxygens of C143 also contribute to electronegativity near the C35 and C36 backbone. (f)–(h) Surface depictions of electrostatic potential calculations for the regions depicted in (c)–(e), respectively.

the Mg1 binding pocket as well as multiple long-range contacts to distal parts of the RNA molecule. We propose that interferences at A101 and A105 do not result from disruption of metal sites but instead from perturbation of contacts between these residues and other M-box regions by the slightly bulkier sulfur groups. Indeed, the pro-R_p oxygen of A101 is positioned within 2.7 Å of the A165 N6 exocyclic amine as well as 2.6 Å to the guanosine 2′ hydroxyl of G22 (Fig. 4b). Disruption of the proper positioning of G22 via phosphorothioate incorporation might be particularly detrimental due to the fact that this nucleotide also makes long-range contacts to A71 of L4. Similarly, the phosphorothioate interference at A105 may be due to disruption of an interaction between the A105 phosphate oxygen and N1 of G100, an interaction that is undoubtedly significant for organization of the unique, magnesium-bound L5 structural fold. Therefore, disruption of the A101 and A105 phosphate interactions are likely to affect both

the formation of the critical Mg1 binding site and the long-range interactions between L5, L4, and P2.

The remaining sites of phosphorothioate interferences (C35, C36, G91, C89, and U119) are likely to result from factors other than simple disruption of important hydrogen-bonding contacts. Intriguingly, these phosphate oxygens cluster together in a common locus within the RNA molecule, near to several important interhelical junctions within the apical portion of the molecule (Fig. 5a and b). Moreover, these phosphate oxygens are oriented in three-dimensional space with neighboring functional groups in a manner that may be consistent with construction of metal-binding pockets. We speculate from these data that these new sites of interferences are important for three previously unidentified metal-binding sites, designated herein as M7–M9.

The candidate M7 binding site is formed, in part, by the U119 pro-R_p oxygen and the pro-S_p oxygens of A117 and A118 (Fig. 4c). All three of these phosphate oxygens are oriented as if coordinating to a missing metal ion. Interestingly, the distances between these phosphate oxygens are similar to the distances observed between inner-sphere magnesium ligands of other metal-binding sites. For example, the average bond distance for inner-sphere ligands of the Mg1–Mg6 metal sites is 2.168 Å,[20] oriented at approximately 90° angles from one another. Therefore, the approximate distance between adjacent inner-sphere ligands in the Mg1–Mg6 binding sites is 3.066 Å and the approximate distance of inner-sphere ligands on opposite sides of the magnesium ion is 4.336 Å. The pro-S_p oxygen of A118 is 3.36 Å and 2.57 Å from phosphate oxygens of A117 and U119, respectively, and the A117 and U119 phosphate oxygens are placed in a convergent orientation, separated by 4.116 Å. There are no other obvious candidate ligands within the putative M7 binding site, and therefore, the remaining three ligands would be expected to be water molecules if, indeed, a magnesium can chelate to this locus. The region corresponding to these residues has been highlighted in a surface representation of the M-box RNA, colored by electrostatic potential (Fig. 4f). The relatively higher electronegativity of this pocket aids speculation that this region might constitute a metal-binding site.

The putative M8 site involves the C89 and G91 pro-R_p oxygens, which appear to be oriented toward a central cavity. It may also be noteworthy that A90 and A87 ribose 2′ oxygens also appear to be oriented toward this pocket, although 2′ ribose oxygens are rare inner-sphere ligands of magnesiums (Fig. 4d and g).

The putative M9 site involves the pro-R_p oxygens of both C35 and C36, which angle toward each other and toward a well-ordered water molecule in the structural model (Fig. 4e and h). It is possible that the interaction with this water could itself be essential or that this molecule could be mediating an outer-sphere coordination between these phosphate oxygens and a missing metal. It is also possible that the water molecule replaces a metal ion that is present transiently during the folding of the RNA molecule. Consistent with the role of these residues as part of an electronegative metal-binding pocket, phosphate groups of 142–144 are also oriented above and point toward the C35–C36 phosphate oxygens.

In total, these data suggest that M-box RNAs utilize a previously unidentified layer of complexity for their metalloregulatory functions. If we are correct in speculating that a subset of the phosphorothioate interferences occur within putative metal-binding pockets (M7–M9), there are multiple potential explanations for the absence of metal ions at these locations in the prior structural model. It is possible that they are only transiently required during RNA folding. Alternatively, their local structural environment may have been perturbed enough during crystallization to result in a loss of metal ion occupancy. Regardless, the observation that phosphorothioate interferences cluster within these three loci provides functional evidence for their role in formation of the compact conformation of M-box RNAs.

Phosphorothioate substitutions in the presence of thiophilic metals

In general, phosphorothioate modifications disrupt magnesium-binding sites due to the fact that hard metals prefer to interact with hard ligands rather than soft ligands (e.g., sulfur).[25] Thiophilic metals prefer interactions with soft ligands but are still usually capable of adopting the octahedral geometry typical for magnesium ions. Therefore, it is a common technique to reassess phosphorothioate interference patterns using RNA molecules that have been incubated in the presence of more 'thiophilic' metals.[31] Rescue of phosphorothioate interferences by thiophilic metals is generally then taken as evidence of restoration of critical metal–RNA contact sites. However, addition of thiophilic metals can also rescue interferences at positions that are not predicted by structural analyses to associate directly with metal ions, suggesting that interpretation of thiophilic 'rescue' data may not always be straightforward.[26]

While the most commonly used metal for thiophilic rescue experiments is manganese, other ions such as cobalt, cadmium, nickel, and zinc are often used.[26,32] In the present study, separation of extended and compacted M-box RNAs was performed in a mixture of 0.5 mM cadmium and 0.5 mM magnesium and analyzed relative to the 1.0 mM magnesium data. A single rescue of a phosphorothioate interference site was observed for G100, one of the positions responsible for coordination of Mg1 (Supplementary Fig. S3). However, sulfur substitutions at the remaining two phosphate oxygens that contact Mg1 (C102 and A103) were not rescued by cadmium. In general, the inability of thiophilic metal ions to rescue sites of phosphorothioate-induced interference cannot be taken as evidence against the presence of a magnesium-binding site. It has been previously noted that phosphorothioate substitutions at established magnesium sites are not always rescued by thiophilic metal ions, possibly due to metal ion exclusion by the bulkier sulfur group.[33,34] It has also been suggested

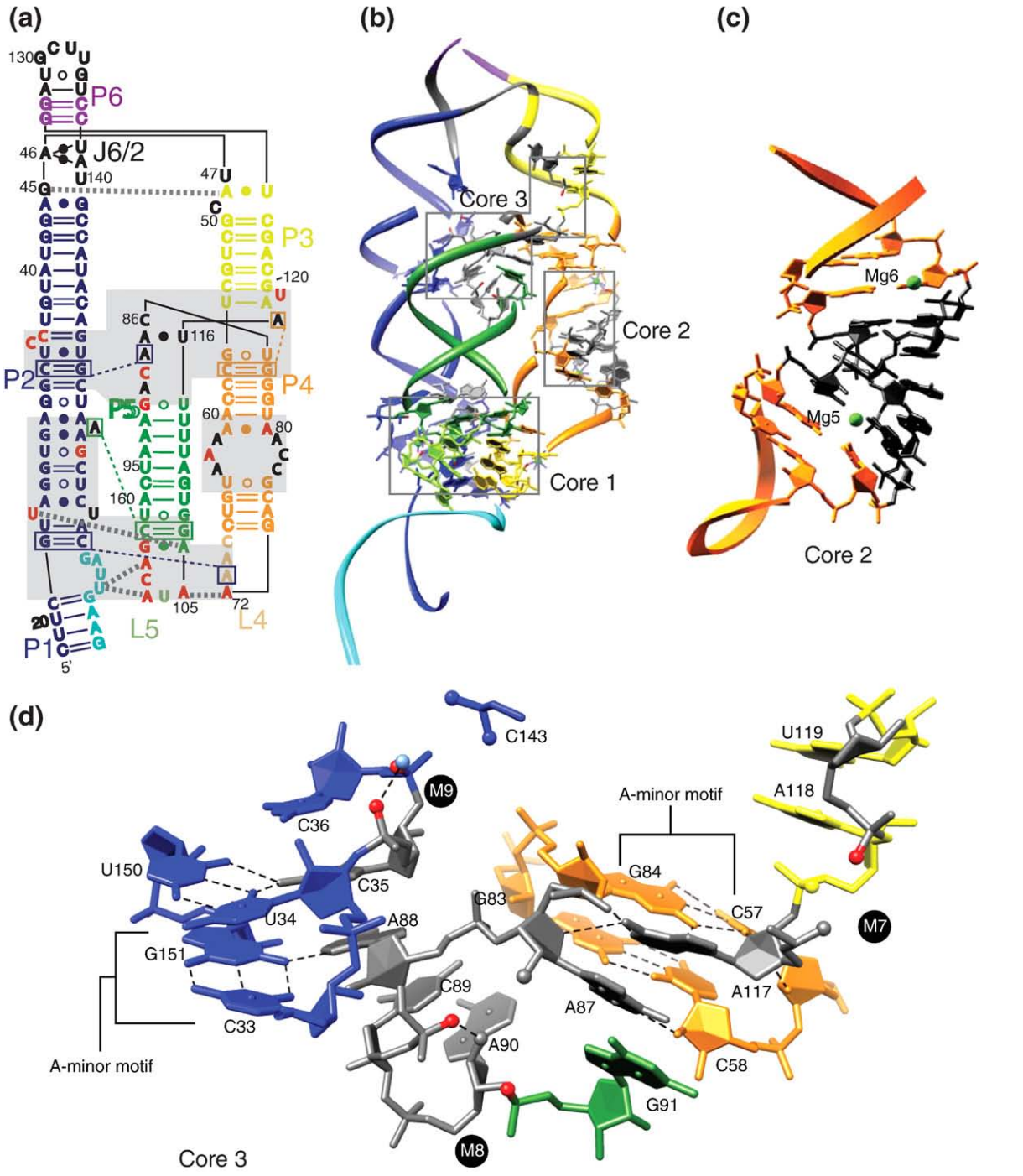

Fig. 5. Metal-binding sites can be grouped into three separate cores. (a) Secondary-structure diagram showing long-range base interactions (dashed lines), A-minor motif interactions (colored boxes connected by dashed lines), sites of phosphorothioate interferences (red letters), and magnesium cores (gray shaded boxes). (b) Residues contacting metals or involved in long-range base interactions are shown within the structural model. These residues cluster within the three magnesium cores postulated herein. (c) The magnesiums of Core 2 assist in orienting bases to stack on either the top or the bottom half of the P4 helix while introducing a kinked orientation of the P4 terminal loop (L4). This orientation is necessary for formation of tertiary contacts between L4, L5, and P2. Observation of phosphorothioate interferences at the Mg5 and Mg6 sites indicates that Core 2 is functionally important. (d) Residues within Core 3. Specific hydrogen-bonding interactions are highlighted with dashed lines. Key A-minor motifs are labeled accordingly. Regions corresponding to the newly identified candidate metal sites (M7–M9) are indicated. These sites appear to assist formation of key tertiary interactions, interhelical bonds, and stacking interactions.

that highly coordinated magnesiums are not easily replaced by thiophilic metals.[26,33] Therefore, the fact that most of the interferences are not rescued by thiophilic metals could be a testament to the high degree to which each individual metal ion is sensed by the M-box RNA.

Discussion

Magnesium-binding sites can be grouped into three 'core' regions

The structural model of the *B. subtilis mgtE* M-box RNA previously revealed the presence of six well-ordered magnesiums[20] but could not address their relative importance for metalloregulatory control. It is not unusual to observe RNA-chelated magnesium; indeed, RNA tertiary structures are oftentimes dependent on magnesium ions that assist in bridging long-range interactions or positioning key residues for tertiary contacts.[2,4,6] Therefore, it was unclear from the M-box structural model alone whether all or a subset of these metals were intricately involved in signal responsiveness. Moreover, other than direct sequestration of nucleotides required for genetic control, it was unclear what features of M-box RNA tertiary structure are unique for their function as metalloregulatory agents. From their large size (>150 nt) and phylogenetic patterns (e.g., extensive primary sequence conservation and widespread phylogenetic distribution), it can be assumed that M-box RNAs exhibit unique structural features that render them as specialized metal sensors as opposed to simple, common structural folds. Our intent in analyzing M-box RNAs is to elucidate these basic mechanistic features and correlate them with the general understanding of bacterial magnesium homeostasis.

The observation that six divalents are directly chelated to M-box RNAs suggested the possibility that intracellular responsiveness to magnesium by M-box RNAs might be exquisitely controlled via a coordinated progression of magnesium-binding sites and metal-induced structural features. The typical riboswitch responds to a single metabolite ligand over a ~100-fold range in concentration, although the cooperative binding of multiple ligands to the glycine riboswitch remains a notable exception.[35] A sharper change in gene expression might be elicited for M-box RNAs in response to even minor magnesium fluctuations if tertiary structure formation is tightly coupled to a highly cooperative network of direct and indirectly associated magnesium ligands. Therefore, identification of metal sites that are essential for function is an important part in elucidating the basic features of M-box regulatory RNAs and their role in control of intracellular magnesium.

Reassessment of the individual roles and importance of the six divalents observed in the structural model (Mg1–Mg6), prompted by the biochemical data presented herein, suggests that they can be grouped into two distinct, functionally related clusters. We have defined these metal-binding 'core' regions based on both the co-localization of magnesium sites and the degree of phosphorothioate interferences for positions within each cluster. Our utilization of this term resembles in concept the metal-binding core located within the P4–P6 domain of the *Tetrahymena* group I intron, which is important for organization of the P5abc subdomain and the subsequent folding pathway.[36] We propose that the separate metal-binding cores within the M-box RNA work in a coordinated manner to accomplish common structural tasks. Mg1–Mg4, located within the tripartite junction in which distal regions of the RNA (P2, L4, and L5) are brought into close proximity with each other, form Core 1, while Mg5 and Mg6, located in a peripheral region of the RNA within a P4 internal loop, constitute Core 2 (Fig. 5a and b).

Proximity of Core 1 to the antiterminator nucleotides and the structural features that sequester them suggested that it might be more significant than Core 2 for formation of the final metal-bound, compacted conformation. Indeed, equally strong phosphorothioate interferences were observed at all but one of the positions involved in formation of the Core 1 binding sites, even at magnesium concentrations above the apparent K_D. The observation that the individual interference strength is similar for each of the positions in Core 1 suggested that they are functionally intertwined (Supplementary Fig. S4). Consistent with this prediction, nucleotides surrounding each magnesium-binding site appear to work together to mediate the formation of multiple long-range contacts. Mg4 and Mg1 bring the P4 and P5 terminal loops (L4 and L5) together by positioning A72 and A105, respectively, which appear to form hydrogen-bonding interactions between their respective N1 and N6 functional groups. Mg1 also positions L5 residues, A101 and A103, for hydrogen-bonding interactions with U167, located within the P2 helix. Together, these interactions anchor L5 and L4 to the base of the molecule. These interactions are further bolstered by an A-minor motif[37] formed between A71 and a P2 G:C base pair, an interaction that is likely to be dependent on the presence of Mg4. Also, Mg2 directly contacts phosphate oxygens from both P2 and L5, while Mg3 assists in positioning P2 residues for long-range hydrogen-bonding interactions to L4. Therefore, the Core 1 metal sites appear to be crucially linked to one another and the final folded architecture of the metal-bound M-box RNA.

Just as Core 1 metal-binding residues shared a similar overall degree of phosphorothioate interferences, so, too, do Core 2 positions (Supplementary Fig. S4). Due to the peripheral location of Core 2, we did not originally expect this region to be as essential as Core 1. Indeed, Core 2 interferences were all classified as weak to moderate interferences for 0.5 mM magnesium and were not observed at 1.0 mM magnesium, suggesting that their functional role(s) may be partially supplanted during conditions of metal excess. Under 0.5 mM magnesium conditions, the A63 contact to Mg5 just meets the criteria for a moderate interference, while the A80 contact to Mg6, the most tangentially associated magnesium, appears as a weak, though reproducible, interference. However, these magnesium sites are both located within an internal loop within the P4 helix where they appear to stabilize base-stacking interactions between residues that stack against the top and bottom half of the P4 helix, respectively (Fig. 5c). A modest kink is introduced between these helices, which in turn

allows for proper orientation of the P4 terminal loop for long-range interactions to L5 and P2. All M-box RNAs that have been identified[38] contain the A-rich P4 internal loop that constitutes Core 2, bolstering the presumption that this structural element and the magnesium that promote it are essential for M-box metalloregulatory function.

The additional sites of phosphorothioate-induced interferences that could not be explained by the existing structural model did not appear to fit into either of these two magnesium cores. Instead, they are all located near the apex of the M-box structure in a cluster that may constitute a third metal-binding core. More specifically, these phosphorothioate interferences cluster together into three separate foci that may constitute individual metal-binding pockets, although there are also alternative explanations of the data. As with Cores 1 and 2, the interference values within the putative Core 3 share a common intensity, suggesting that the putative individual metal sites may be working in conjunction with one another (Supplementary Fig. S4). Correspondingly, analysis of the Core 3 putative metal-binding sites revealed that, as in Core 1, surrounding nucleotides appear to be positioned for formation of long-range base contacts. While Core 1 functions to stabilize the tripartite interaction between the three parallel P2, P4, and P5 helices at the base of the molecule, Core 3 appears to stabilize the tripartite interaction at the opposing end of the molecule (Fig. 5a, b, and d). Each of the individual putative metal sites (M7–M9) within Core 3 appears to individually promote formation of essential long-range contacts. For example, the putative M8 binding site that is formed in part by C89 and G91 appears to assist in positioning the adjacent nucleotides (A87 and A88) such that they splay out in opposite directions, thereby allowing long-range hydrogen-bonding interactions with nucleotides that participate in formation of the other two putative metal sites, M7 and M9. The adenine nucleobase of A117, one of the nucleotides whose phosphate oxygen participates in formation of the M7 site, forms a base-stacking interaction with A87 while simultaneously forming an A-minor motif interaction with a P4 G:C base pair, thereby linking P4 and P5 through tertiary interactions. A88 forms base-stacking interactions with its adjacent nucleotides C89 and A90 as well as C35, a bulged nucleotide within the P2 helix whose phosphate oxygen participates with formation of the putative M9 site in conjunction with C36. This contact forms one link between the P2 and P5 helices while yet another contact is created by formation of an A-minor motif between A88 and a base pair of the P2 helix. Indeed, all four A-minor motif interactions and most other long-range interactions observed in the structural model appear to be dependent on metal-binding sites in Core 1 and the putative Core 3 (Figs. 3 and 5). Therefore, our data suggest that the network of three helical, long-range contacts required for stabilization of the compact RNA conformation is likely to be dependent on metal-binding sites at the base of the molecule (Core 1) and at the top of the molecule (Core 3). Presumably, it is the coordinated action of these structural features that has, in part, engendered the basic physical properties of the M-box tertiary fold to allow it to function as a dedicated metal sensor in bacteria.

While it is tempting to designate the electronegative pockets that contain sites of phosphorothioate interferences as putative metal-binding sites, alternative explanations must also be considered. It is possible that hydronium ions or hydrogen-bonding networks could satisfy the electronegative charge that accumulates within the M7–M9 pockets, rather than through association with metal ions. Phosphorothioate interferences could also result from perturbation of individual hydrogen-bonding interactions.[39,40] While this outcome of phosphorothioate substitutions is likely to be responsible for interferences observed at A101 and A105, the structural model does not reveal any obvious interactions that could be disrupted by sulfur substitutions at C35, C36, C89, G91, or U119. However, we cannot rule out the possibility that these substitutions affect hydrogen bonds that are specifically important during the RNA folding process but are not present in the final native structure. It is also important to note that the charge distribution around the phosphate group is altered upon phosphorothioate substitution.[41] A greater proportion of the negative charge becomes distributed toward the remaining nonbridging oxygen for phosphorothioate-containing linkages. This could affect folding pathways by altering local electrostatic interactions between backbone phosphates. Finally, it is also possible that the larger radius of sulfur relative to oxygen might lead to deleterious steric effects. Further biochemical and structural analyses will be required to fully resolve the role(s) of residues within the putative Core 3 during metal-induced folding of M-box RNAs. Nonetheless, it is clear from the data presented herein that backbone oxygens within the Core 3 region are equally important to the metal-binding sites observed in the structural model and within Cores 1 and 2.

Materials and Methods

RNA preparation

DNA templates for RNA transcription were prepared via PCR in which the T7 promoter sequence was incorporated into the forward primer. For wild-type RNAs, the DNA template was amplified from *B. subtilis* IA40 chromosomal DNA (Bacillus Genetic Stock Center, Columbus, OH). The primers were designed to amplify positions corresponding to nucleotides 14–172 relative to the transcriptional start site of the *B. subtilis mgtE* gene. For M3 mutant RNAs, the DNA template was amplified from a plasmid containing a version of the M-box in which nucleotides 107–109 had been mutated from GGU to CCA. Wild-type and M3 RNAs were synthesized *in vitro* at 37 °C in 25- to 50-μl reaction mixtures that included 10–30 pmol DNA templates, 30 mM Tris–HCl (pH 8.0), 10 mM DTT, 0.1% Triton X-100, 0.1 mM spermidine–HCl, 2.5–5.0 mM of each NTP (Roche), 40 mM $MgCl_2$, and ~50 μg mL^{-1} T7 RNA polymerase. Reactions were terminated after 2.5 h with 2× volume 8 M urea. Products

were resolved by 6% denaturing PAGE, and RNA-containing bands were excised, cut into ~1-mm cubes, and equilibrated in 200 mM NaCl, 10 mM Tris–HCl (pH 7.5), and 10 mM ethylenediaminetetraacetic acid (EDTA) (pH 8.0) for <2 h at 23 °C. The passively eluted RNAs were ethanol precipitated, resuspended in water, quantified at A_{260}, and utilized as markers during nondenaturing gel electrophoresis.

M-box RNAs with randomly incorporated phosphorothioate modifications were transcribed in 1-mL reaction mixtures that included 0.5–1 nmol DNA template, 30 mM Tris–HCl (pH 8.0), 10 mM DTT, 0.1% Triton X-100, 0.1 mM spermidine–HCl, 1 mM of each NTP (Roche), 40 mM $MgCl_2$, ~50 μg mL^{-1} T7 RNA polymerase, 1 U of yeast inorganic pyrophosphatase (Sigma), and 50 μM ATPαS, 100 μM CTPαS, 50 μM GTPαS, or 50 μM UTPαS (Glen Research). The levels of nucleotide analogues added to the transcription reactions were chosen for ~5% incorporation overall, allowing for single phosphorothioate substitutions.[31,40] Reactions were terminated after 2.5 h with the addition of 1-mL buffered phenol, followed by extraction with phenol/chloroform. The RNA transcripts were ethanol precipitated and resuspended in 125 μL water. One hundred microliters was removed for size-exclusion chromatography (conducted at room temperature) and subsequent nondenaturing gel electrophoresis (resolved at approximately 4 °C). The remaining RNA was retained for use as the unselected, parent RNA pool to which the extended and compacted RNA molecules were compared.

Size-exclusion chromatography

All chromatography experiments were performed at room temperature using an 18-1900-26 ÄKTA™ FPLC and a Superdex 200 10/300 GL column with a flow rate of 0.5 mL/min. Fractions were collected in 0.5-mL increments. The running buffer contained 10 mM Tris–HCl (pH 7.5), 100 mM KCl, and either 1 mM or 0.5 mM $MgCl_2$. Fractions corresponding to the extended and compacted RNA species were collected, concentrated, and radioactively labeled at the 5′ terminus prior to separation by nondenaturing PAGE.

Nondenaturing PAGE

All RNAs were dephosphorylated using calf intestinal alkaline phosphatase (New England Biolabs), 5′-radiolabeled using T4 polynucleotide kinase (New England Biolabs) and [γ-^{32}P]ATP (Amersham), and resolved by 6% denaturing gel electrophoresis. Radiolabeled RNAs were then excised; passively eluted into 200 mM NaCl, 10 mM Tris–HCl (pH 7.5), and 10 mM EDTA (pH 8.0); ethanol precipitated; and resuspended in RNase-free water. Eight percent nondenaturing polyacrylamide gels (29:1 acrylamide/bisacrylamide) were prepared with 1 mM $MgCl_2$, 0.5 mM $MgCl_2$, or a mixture of 0.5 mM $MgCl_2$ and 0.5 mM $CdCl_2$ and Tris–borate buffer containing the same metal ion concentrations. Samples were electrophoresed at a constant 20 W for 4 h at 4 °C. RNA-containing bands were visualized by autoradiography, excised, cut into ~1-mm cubes, and then equilibrated in 200 mM NaCl, 10 mM Tris–HCl (pH 7.5), and 10 mM EDTA (pH 8.0) for <2 h at 23 °C. These passively eluted RNAs were then ethanol precipitated and resuspended in water to approximately match 100,000 cpm/μL, as verified by scintillation counting.

Visualization and quantitation of phosphorothioate interferences

The four individual RNA pools, resulting from incorporation of ATPαS, CTPαS, GTPαS, or UTPαS and radiolabeled with ^{32}P at the 5′ terminus, were matched by scintillation counting. Specifically, two aliquots of 500,000 cpm RNA were each resuspended in 8 μL of water and 1 μL of yeast total RNA (Ambion). Cleavage at phosphorothioate substitutions was induced for one of the aliquots via addition of 1 μL of 100 μM iodine dissolved in ethanol. One microliter of water was added to the second aliquot as a control population for background cleavages. Five microliters of 3× formamide loading buffer (95% formamide, 20 mM EDTA, 0.01% bromophenol blue, and 0.01% xylene cyanol) was added to each tube and the reactions were heated to 95 °C for 2 min prior to resolution by 10% denaturing PAGE. The resulting gels were dried and analyzed by phosphorimaging instrumentation (Molecular Dynamics Typhoon) and phosphor storage screens (Amersham).

Individual band intensities were quantified using semi-automated footprinting analysis (SAFA)[42] and ImageQuant software (Molecular Dynamics) via standard methodology. Individual bands corresponding to sites of random phosphorothioate substitutions were quantified by SAFA both for untreated RNA pools and those that were subjected to iodine-mediated oxidation. Background intensities (resulting from analysis of untreated RNAs) were subtracted from band intensities for iodine-treated RNAs. Preliminary interference values were obtained by dividing the values measured for the parental (unselected) pool by values measured for individual selected pools. These data were normalized to account for minor variations in loading. This was accomplished by calculating a mean value from all positions within a particular data set, excluding a small subset of positions whose interference values were greater than 5 or less than 0.2. All values within a given data set were divided by the average of values falling within 1 SD of this mean. The resulting interference values were arbitrarily deemed strong if they exceeded 10, moderate if they exceeded 5, and weak if they exceeded 2. Similar analyses of phosphorothioate incorporation experimentation are reported elsewhere.[23,43] All data shown in this paper are quantified from the average of at least two independent experiments.

Nucleotides 128–170 could not easily be analyzed using SAFA alone due to the fact that these regions were not well resolved; therefore, these regions were compared using line trace software in ImageQuant, and any positions showing potential interferences were analyzed by individual band boxing quantification. Also, increased levels of background cleavages at positions A25, A48, A70, A79, C86–A90, and C102–A106 obscured analyses of these positions for the extended RNAs to varying degrees, but analyses of compacted RNAs remained relatively free of background and were therefore analyzed at all positions.

Structural figures were generated using UCSF Chimera.[44] Electrostatic potential calculations were done using APBS[45] as described by Stahley *et al.*[46] with the input files for APBS prepared using pdb2pqr.[47] Visualization of electrostatic potentials on the surface of the M-box crystal structure was done using Pymol[48] with the APBS plugin.

Acknowledgements

Molecular graphics images were produced using the UCSF Chimera package from the Resource for

Biocomputing, Visualization, and Informatics at the University of California, San Francisco. Research on metal-responsive riboswitches in the Winkler laboratory is funded primarily by NIH grant GM081882 with additional support from the Welch Foundation (I-1643) and The University of Texas Southwestern Medical Center Endowed Scholars Program.

Supplementary Data

Supplementary data associated with this article can be found, in the online version, at doi:10.1016/j.jmb.2009.07.033

References

1. Draper, D. E., Grilley, D. & Soto, A. M. (2005). Ions and RNA folding. *Annu. Rev. Biophys. Biomol.* **34**, 221–243.
2. Woodson, S. A. (2005). Metal ions and RNA folding: a highly charged topic with a dynamic future. *Curr. Opin. Chem. Biol.* **9**, 104–109.
3. Sigel, R. K. & Pyle, A. M. (2007). Alternative roles for metal ions in enzyme catalysis and the implications for ribozyme chemistry. *Chem. Rev.* **107**, 97–113.
4. Draper, D. E. (2008). RNA folding: thermodynamics and molecular descriptions of the roles of ions. *Biophys. J.* **95**, 5489–5495.
5. Chu, V. B., Bai, Y., Lipfert, J., Herschlag, D. & Doniach, S. (2008). A repulsive field: advances in the electrostatics of the ion atmosphere. *Curr. Opin. Chem. Biol.* **12**, 619–625.
6. Klein, D. J., Moore, P. B. & Steitz, T. A. (2004). The contribution of metal ions to the structural stability of the large ribosomal subunit. *RNA*, **10**, 1366–1379.
7. Wakeman, C. A., Winkler, W. C. & Dann, C. E. (2007). Structural features of metabolite-sensing riboswitches. *Trends Biochem. Sci.* **32**, 415–424.
8. Schwalbe, H., Buck, J., Furtig, B., Noeske, J. & Wohnert, J. (2007). Structures of RNA switches: insight into molecular recognition and tertiary structure. *Angew. Chem., Int. Ed. Engl.* **46**, 1212–1219.
9. Montange, R. K. & Batey, R. T. (2008). Riboswitches: emerging themes in RNA structure and function. *Annu. Rev. Biophys.* **37**, 117–133.
10. Cochrane, J. C. & Strobel, S. A. (2008). Riboswitch effectors as protein enzyme cofactors. *RNA*, **14**, 993–1002.
11. Roth, A. & Breaker, R. R. (2009). The structural and functional diversity of metabolite-binding riboswitches. *Annu. Rev. Biochem.* **78**, 305–334.
12. Mironov, A. S., Gusarov, I., Rafikov, R., Lopez, L. E., Shatalin, K., Kreneva, R. A. *et al.* (2002). Sensing small molecules by nascent RNA: a mechanism to control transcription in bacteria. *Cell*, **111**, 747–756.
13. Winkler, W. C., Cohen-Chalamish, S. & Breaker, R. R. (2002). An mRNA structure that controls gene expression by binding FMN. *Proc. Natl Acad. Sci. USA*, **99**, 15908–15913.
14. Winkler, W. C., Nahvi, A. & Breaker, R. R. (2002). Thiamine derivatives bind messenger RNAs directly to regulate bacterial gene expression. *Nature*, **419**, 952–956.
15. Collins, J. A., Irnov, I., Baker, S. & Winkler, W. C. (2007). Mechanism of mRNA destabilization by the *glmS* ribozyme. *Genes Dev.* **21**, 3356–3368.
16. Cheah, M. T., Wachter, A., Sudarsan, N. & Breaker, R. R. (2007). Control of alternative RNA splicing and gene expression by eukaryotic riboswitches. *Nature*, **447**, 497–500.
17. Wachter, A., Tunc-Ozdemir, M., Grove, B. C., Green, P. J., Shintani, D. K. & Breaker, R. R. (2007). Riboswitch control of gene expression in plants by splicing and alternative 3′ end processing of mRNAs. *Plant Cell*, **19**, 3437–3450.
18. Dambach, M. D. & Winkler, W. C. (2009). Expanding roles for metabolite-sensing regulatory RNAs. *Curr. Opin. Microbiol.* **12**, 161–169.
19. Cromie, M. J., Shi, Y., Latifi, T. & Groisman, E. A. (2006). An RNA sensor for intracellular Mg^{2+}. *Cell*, **125**, 71–84.
20. Dann, C. E., Wakeman, C. A., Sieling, C. L., Baker, S. C., Irnov, I. & Winkler, W. C. (2007). Structure and mechanism of a metal-sensing regulatory RNA. *Cell*, **130**, 878–892.
21. Mandal, M., Lee, M., Barrick, J. E., Weinberg, Z., Emilsson, G. M., Ruzzo, W. L. & Breaker, R. R. (2004). A glycine-dependent riboswitch that uses cooperative binding to control gene expression. *Science*, **306**, 275–279.
22. Strobel, S. A. & Shetty, K. (1997). Defining the chemical groups essential for *Tetrahymena* group I intron function by nucleotide analog interference mapping. *Proc. Natl Acad. Sci. USA*, **94**, 2903–2908.
23. Ryder, S. P. & Strobel, S. A. (1999). Nucleotide analog interference mapping. *Methods*, **18**, 38–50.
24. Waldsich, C. (2008). Dissecting RNA folding by nucleotide analog interference mapping (NAIM). *Nat. Protoc.* **3**, 811–823.
25. Eckstein, F. (1985). Nucleoside phophorothioates. *Annu. Rev. Biochem.* **54**, 367–402.
26. Basu, S. & Strobel, S. A. (1999). Thiophilic metal ion rescue of phosphorothioate interference within the *Tetrahymena* ribozyme P4–P6 domain. *RNA*, **5**, 1399–1407.
27. Waring, R. B. (1989). Identification of phosphate groups important to self-splicing of the *Tetrahymena* rRNA intron as determined by phosphorothioate substitution. *Nucleic Acids Res.* **17**, 10281–10293.
28. Gish, G. & Eckstein, F. (1988). DNA and RNA sequence determination based on phosphorothioate chemistry. *Science*, **240**, 1520–1522.
29. Griffiths, A. D., Potter, B. V. L. & Eperon, I. C. (1987). Stereospecificity of nucleases towards phosphorothioate-substituted RNA: stereochemistry of transcription by T7 polymerase. *Nucleic Acids Res.* **15**, 4145–4162.
30. Horton, T. E., Maderia, M. & DeRose, V. J. (2000). Impact of phosphorothioate substitutions on the thermodynamic stability of a RNA GAAA tetraloop: an unexpected stabilization. *Biochemistry*, **39**, 8201–8207.
31. Christian, E. L. & Yarus, M. (1993). Metal coordination sites that contribute to structure and catalysis in the group I intron for *Tetrahymena*. *Biochemistry*, **32**, 4475–4480.
32. Weinstein, L. B., Jones, B. C. N. M., Cosstick, R. & Cech, T. R. (1997). A second catalytic metal ion in a group I ribozyme. *Nature*, **388**, 805–808.
33. Brautigam, C. A. & Steitz, T. A. (1998). Structural principles for the inhibition of the 3′–5′ exonuclease activity of *Escherichia coli* DNA polymerase I by phosphorothioates. *J. Mol. Biol.* **277**, 363–377.
34. Ruffner, D. E. & Uhlenbeck, O. C. (1990). Thiophosphate interference experiments locate phosphates important for the hammerhead RNA self cleavage reaction. *Nucleic Acids Res.* **18**, 6025–6029.

35. Welz, R. & Breaker, R. R. (2007). Ligand binding and gene control characteristics of tandem riboswitches in *Bacillus anthracis*. *RNA*, **13**, 573–582.
36. Cate, J. H., Hanna, R. L. & Doudna, J. A. (1997). A magnesium ion core at the heart of a ribozyme domain. *Nat. Struct. Biol.* **4**, 553–558.
37. Nissen, P., Ippolito, J. A., Ban, N., Moore, P. B. & Steitz, T. A. (2001). RNA tertiary interactions in the large ribosomal subunit: the A-minor motif. *Proc. Natl Acad. Sci. USA*, **98**, 4899–4903.
38. Griffiths-Jones, S., Moxon, S., Marshall, M., Khanna, A., Eddy, S. R. & Bateman, A. (2005). Rfam: annotating non-coding RNAs in complete genomes. *Nucleic Acids Res.* **33**, D121–D124.
39. Hinrichs, W., Steifa, M., Saenger, W. & Eckstein, F. (1987). Absolute configuration of *R*p-uridine 3′,5′-cyclic phosphorothioate. *Nucleic Acids Res.* **15**, 4945–4955.
40. Christian, E. L. & Yarus, M. (1992). Analysis of the role of phosphate oxygens in the group I intron from *Tetrahymena*. *J. Mol. Biol.* **228**, 743–758.
41. Frey, P. A. & Sammons, R. D. (1985). Bond order and charge localization in nucleoside phosphorothiates. *Science*, **228**, 541–545.
42. Das, R., Laederach, A., Pearlman, S., Herschlag, D. & Altman, R. (2005). SAFA: Semi-automated footprinting analysis software for high-throughput quantification of nucleic acid footprinting experiments. *RNA*, **11**, 344–354.
43. Jansen, J. A., McCarthy, T. J., Soukup, G. A. & Soukup, J. K. (2006). Backbone and nucleobase contacts to glucosamine-6-phosphate in the *glmS* ribozyme. *Nat. Struct. Mol. Biol.* **13**, 517–523.
44. Pettersen, E. F., Goddard, T. D., Huang, C. C., Couch, G. S., Greenblatt, D. M., Meng, E. C. & Ferrin, T. E. (2004). UCSF Chimera—a visualization system for exploratory research and analysis. *J. Comput. Chem.* **25**, 605–612.
45. Baker, N. A., Sept, D., Joseph, S., Holst, M. J. & McCammon, J. A. (2001). Electrostatics of nanosystems: application to microtubules and the ribosome. *Proc. Natl Acad. Sci. USA*, **98**, 10037–10041.
46. Stahley, M. R., Adams, P. L., Wang, J. & Strobel, S. A. (2007). Structural metals in the group I intron: a ribozyme with a multiple metal ion core. *J. Mol. Biol.* **372**, 89–102.
47. Dolinsky, T. J., Nielsen, J. E., McCammon, J. A. & Baker, N. A. (2004). PDB2PQR: an automated pipeline for the setup of Poisson–Boltzmann electrostatics calculations. *Nucleic Acids Res.* **32**, 665–667.
48. Delano, W. L. (2002). *The PyMOL Molecular Graphics System.* DeLano Scientific, San Carlos, CA.